

Towards Domain Generalization in Object Detection

Xingxuan Zhang¹, Zekai Xu¹, Renzhe Xu¹, Jiashuo Liu¹, Peng Cui^{1*},
Weitao Wan², Chong Sun², Chen Li²

¹Department of Computer Science, Tsinghua University ²WeChat, Tencent Inc.

xingxuanzhang@hotmail.com, xuzk20@mails.tsinghua.edu.cn, xrz199721@gmail.com,
liujiashuo77@gmail.com, cuiip@tsinghua.edu.cn, collinwan@tencent.com,
waynecsun@tencent.com, chaselli@tencent.com

Abstract

Despite the striking performance achieved by modern detectors when training and test data are sampled from the same or similar distribution, the generalization ability of detectors under unknown distribution shifts remains hardly studied. Recently several works discussed the detectors' adaptation ability to a specific target domain, which are not readily applicable in real-world applications since detectors may encounter various environments or situations while pre-collecting all of them before training is inconceivable. In this paper, we study the critical problem, domain generalization in object detection (DGOD), where detectors are trained with source domains and evaluated on unknown target domains. To thoroughly evaluate detectors under unknown distribution shifts, we formulate the DGOD problem and propose a comprehensive evaluation benchmark to fill the vacancy. Moreover, we propose a novel method named Region Aware Proposal reweighTing (RAPT) to eliminate dependence within RoI features. Extensive experiments demonstrate that current DG methods fail to address the DGOD problem and our method outperforms other state-of-the-art counterparts.

1. Introduction

Modern detectors have shown striking performance when trained and tested with data sampled from a single benchmark [93], yet many application scenarios require reliable and stable performance when encountered input data from any possible distribution including those differs from the distribution of training data [48, 72, 91, 107]. For example, autonomous driving requires all vehicles, pedestrians and signal lights to be accurately detected under any distribution shifts caused by inconsistency in contexts, time,

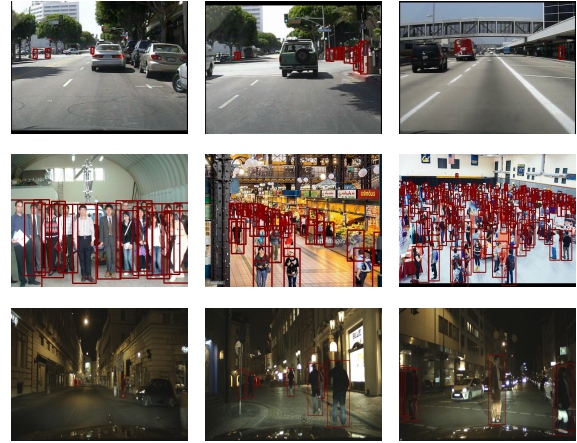


Figure 1. Comparison of Caltech [15], CrowdHuman [70], and ECP [4]. Clear distribution shifts are introduced by the density of people, image contexts, illumination and filming anchors.

weather, shot angle and illumination [9, 26].

Since significant distribution shifts are among real-world detection data (as shown in Fig. 1) and pre-collected data can hardly involve all of the possible situations in real-world applications, the generalization ability of models to unseen distributions is critical for detectors. Thus training and testing detectors with data sampled from a given dataset lack evaluation significance for practical applications, yet detectors may suffer from significant performance drops under simple disturbance [9, 25]. This situation brings a critical question: how to improve the generalization ability of modern detectors and how to thoroughly evaluate them towards real-world applications in unknown scenes.

Some works studied the domain adaptation (DA) problem in object detection to improve models' performance on a domain with limited category and bounding box annotations, where the distribution of test images is accessible in the training phase [24, 31, 33], and showed promising results. However, as mentioned above, under the cir-

*Corresponding author

cumstances where one can hardly ensure the availability of test data distribution domain adaptation methods cannot be readily applied [71].

Despite the urgent need of the evaluation of detectors under unknown distribution shifts for real-world applications, recent literature lacks the discussions of evaluation methods and evaluation metrics for the object detection problem under distribution shifts. In this paper we formulate the problem of object detection under distribution shifts and propose a evaluation method with multiple detection datasets for it. To thoroughly evaluate generalization ability [18, 42, 54], none of the prior knowledge of test distribution is available in the training phase.

Recently considerable attention has been drawn to the field of domain generalization (DG) for image recognition [69, 72, 79]. Specifically, in the DG literature [72, 80, 103], a category is split into multiple domains according to data source [78], context [29], or image style [39], so that domain-related features (e.g., features that are irrelevant to categories, such as features of image style, figure resolution, etc.) vary across different domains while category relevant features remain invariant. Such a split of heterogeneous data makes it possible for a well-designed model to learn the invariant representations across domains and inhibit the negative effect from domain-related features, leading to better generalization ability under distribution shifts [98].

Moreover, inspired by DG evaluation approaches [39, 57], we propose a comprehensive cross-dataset evaluation protocol to test the generalization ability of detectors. Different from [25], which mainly focuses on adaptation between two given datasets and progressive fine-tuning, we introduce four kinds of distribution shifts via clustering several large-scale benchmarks into two groups for training and evaluation, respectively. These settings, namely *classic DG*, *density shift*, *context shift*, and *random shift*, evaluate detection robustness against diverse distribution shifts with practical meaning and significant impact. With extensive experiments, we show that RAPT improves the generalization ability of detectors under various distribution shifts.

Essentially, model crash under distribution shifts is mainly induced by the spurious correlations between domain-related features and category labels, which are intrinsically caused by the subtle correlations between relevant and irrelevant features [1, 37, 50, 53, 98]. Consider the context in street detection scenarios as an example, if pedestrians are usually on the sidewalk in the training data, there are strong spurious correlations between features of sidewalk and the label ‘person’. When tested with images where pedestrians are not on the sidewalk (such as on the road), detectors may yield wrong predictions. Significant drops in performance are caused by the difference in context between training and testing data [29, 98], as shown in Section 4.

Some recent works have proposed to decorrelate relevant features and irrelevant features with sample reweighting and shown effectiveness [36, 71, 98]. Nevertheless, most of them focus on simple data structures (e.g., linear models [36, 71]) or basic tasks (e.g., image classification [98]).

In object detection, however, one single image can yield many proposals and predictions, leading to insufficient learning of sample weights for images. Thus we propose a novel sample reweighting method called Region Aware Proposal reweighTing (RAPT) to learn weights for proposals to eliminate the statistical dependence between features. Since RoI features are of high dimensions, which introduces enormous calculation, RAPT clusters proposals according to their visible features and the relative position of the visible area, and learns sample weights within each cluster. In this manner, the spatial knowledge of RoI features and visible parts is leveraged for prediction while computational complexity is small enough to be ignored.

2. Related Works

Object detection and pedestrian detection Object detection aims to learn accurate detectors for various categories. There are two mainstreams for object detection: single-stage detectors [2, 44, 46, 63, 64, 77] and two-stage detectors [13, 43, 65, 87]. The main difference of them lies in whether the proposes are filtered through second stage heads. Most of them adopt rectangular anchors for the object representation, while some of recent works proposed to present objects in terms of point sets [16, 38, 83, 87, 88, 105] and achieved comparable performance compared with rectangular anchors based ones. Pedestrian detection is a sub-field of object detection, which is prone to be effected with distribution shifts and it requires highly reliable detectors. Thus we consider pedestrian detection as one of our evaluation scenarios. Many modern pedestrian detection methods [11, 30, 47, 67, 81, 92, 94] are inspired by standard object detection, such as Faster RCNN [65], RetinaNet [44] and Single Shot MultiBox Detector (SSD) [46]. Recently, the occlusion problem in pedestrian detection has drawn lots of attention. To tackle this problem, penalty based methods [82, 96] are proposed to force the detector to focus on the true target. Some methods also try to adopt visible information as external guidance to learn various occlusion patterns in crowd scenarios [56, 97, 101]. But none of current detectors consider the robustness of pedestrian detectors under distribution shifts.

Domain Generalization With access to data from several source domains, Domain Generalization (DG) problems aim to learn models that generalize well on unseen target domains, which focuses mostly on computer vision related classification problems on the grounds that predictions are prone to be affected by disturbance on images (e.g.,

style, light, rotation, etc.). According to [72], regarding to different methodological focuses, DG methods can be categorized into three branches, namely representation learning [18, 42, 54, 54, 74], training strategy [7, 40, 76, 86, 98, 99, 102] and data augmentation [58, 59, 69, 79, 90, 104]. Existing surveys of this field can be found in [72, 80, 103].

Domain Adaptation in Object Detection Domain adaptation (DA) aims to improve models' performance on a known target domain [49, 66]. Following the basic approach in DA, DA [10] and MTOR [5] minimize domain discrepancy for object detection. SWDA [68] aligns local similar features strongly and aligns global dissimilar features weakly. IFAN [106] aligns feature distributions at both image and instance levels. And other works [24, 84, 89, 100] also show promising performance when the distribution of the target domain is accessible in the training phase, which are not applicable in domain generalization (DG) scenarios where the information of test data is completely inaccessible. Although the domain adaptation in object detection is widely discussed, domain generalization in object detection remains unstudied.

3. Methods

In most current anchor-based detection methods, the significance of each proposal for loss calculation is considered equally. Though several approaches [44, 73] highlight the contribution of hard samples to address the imbalance between categories or foreground and background, they fail to consider the possible heterogeneity and distribution shifts between training and testing data. We propose an effective sample reweighting method called Region-Aware Proposal reweighTing (RAPT) to improve detectors' generalization ability under distribution shifts. RAPT eliminates statistical dependences between relevant features (i.e., features related to the target object) and irrelevant features (i.e., features that vary in different datasets), and thus spurious correlations between irrelevant features and labels are eliminated. As shown in Figure 2, the main idea of RAPT is to consider proposals as samples and learn sample weights to reweight losses generated by corresponding proposals. We give the formulations and theoretical explanations in Section 3.3 and training protocol in Section 3.4.

3.1. Problem Formulation

Notations Let $\mathcal{X} \subseteq \mathbb{R}^{H^{\text{raw}} \times W^{\text{raw}} \times C^{\text{raw}}}$ denote the space of raw pixels with width W^{raw} , height H^{raw} , and number of channel C^{raw} , $\mathcal{Y} \subseteq \mathbb{R}$ denote the space of labels, $\mathcal{B} \in \mathbb{R}^4$ denote the space of bounding boxes. A sample $Q_i = \left\{ X_i, \{y_{ij}, B_{ij}\}_{j=1}^{N_i} \right\}$ with index i includes image $X_i \in \mathcal{X}$ and N_i pairs of category labels $y_{ij} \in \mathcal{Y}$ and bounding boxes $B_{ij} \in \mathcal{B}$.

Let \mathcal{E} be the set of all possible domains and a specific domain $e \in \mathcal{E}$ corresponds to a distribution P^e on the space of sample Q . Let $\mathcal{E}_{\text{tr}} \subseteq \mathcal{E}$ be the set of all training domains. For any training domain $e \in \mathcal{E}_{\text{tr}}$, let $D_e = \{Q_i\}_{i=1}^{N_e}$ be the training data with N_e samples drawn from P^e . In addition, there exists an unknown testing domain $e_{\text{te}} \in \mathcal{E}$.

We assume that a object detection model $f : \mathcal{X} \rightarrow ((\mathcal{Y} \cup \{\phi\}) \times \mathcal{B})^A$ yield at most A bounding boxes and category predictions from each image. For a model f , let $\mathcal{M}(Q; f)$ be an evaluation metric on sample Q (such as mAP and MR⁻²) to measure the model performance.

Problem 1 (Domain Generalization in Object Detection (DGOD)). Given the training data $\{D_e\}_{e \in \mathcal{E}_{\text{tr}}}$ without domain labels and the evaluation metric \mathcal{M} , the target is to maximize the evaluation metric on the unseen testing domain e_{te} , i.e., $\mathbb{E}_{Q \sim P^{e_{\text{te}}}} [\mathcal{M}(Q; f)]$.

3.2. Overall framework

Let $\mathcal{Z}^{\text{rep}} \subseteq \mathbb{R}^{H^{\text{rep}} \times W^{\text{rep}} \times C^{\text{rep}}}$ denote the space of visual feature maps and $\mathcal{Z}^{\text{RoI}} \subseteq \mathbb{R}^{H^{\text{RoI}} \times W^{\text{RoI}} \times C^{\text{RoI}}}$ denote the space of RoI features. Let $[K]$ denote the set $\{1, 2, \dots, K\}$.

In a anchor based detector, given an image sample X_i , the visual feature map Z_i^{rep} is generated by a backbone representation function $f_{\text{rep}} : \mathcal{X} \rightarrow \mathcal{Z}^{\text{rep}}$. A region proposal network (RPN) $f_{\text{RPN}} : \mathcal{Z}^{\text{rep}} \rightarrow \Delta_{\mathcal{B}}$ is then adopted to generate a distribution on \mathcal{B} and samples N_{pro} proposals $\{B_{ij}^{\text{pro}} \in \mathcal{B}\}_{j=1}^{N_{\text{pro}}}$ from the distribution. Here $\Delta_{\mathcal{B}}$ denotes the space of all distributions on \mathcal{B} .

To regularize the size of features input into the following heads in modern detectors, a RoI pooling function $h_{\text{RoI}} : \mathcal{B} \times \mathcal{Z}^{\text{rep}} \rightarrow \mathcal{Z}^{\text{RoI}}$, such as RoI pooling [21], aligned RoI pooling [27] and deformable RoI pooling [13] is adopted to generate the RoI features Z_{ij}^{RoI} of each proposal for the final predicting function $f_{\text{pred}} : \mathcal{Z}^{\text{RoI}} \rightarrow \mathcal{Y} \times \mathcal{B}$ to generate bounding box regression \hat{y}_{ij} and \hat{B}_{ij} of proposals.

3.3. Region-Aware Proposal Weights Learning

Though sample reweighting based decorrelation methods show effectiveness in regression and classification tasks [71, 98], applying proposal reweighting in detectors suffers major problems.

RoI features Z^{RoI} still maintain the spatial dimension, where similar features may lead to variant instructions for class and bounding box prediction (e.g., human head related features give different instructions to the regression of the bounding box when detected on the right or left of the feature map). Thus eliminating dependences between category relative and irrelevant features requires decorrelations between features within each bin of the RoI feature.

Since decorrelating all the features inside each bin of RoI features of each input image introduces excessive calculation, we propose a region-based proposal reweighting

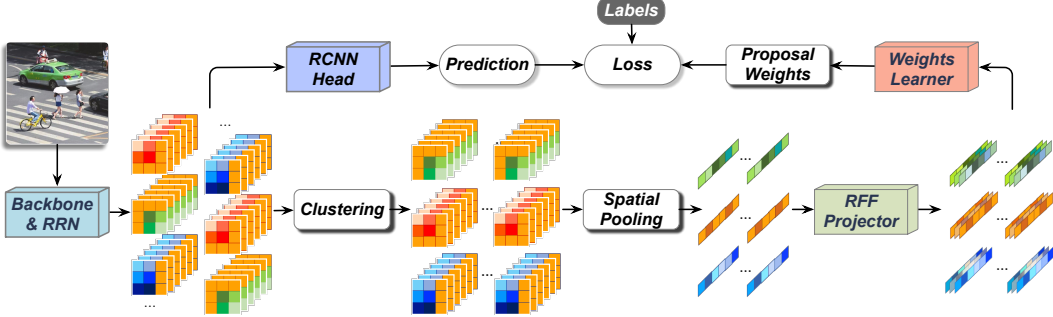


Figure 2. The overall architecture of the proposed RAPT method. The Clustering module clusters Roi features according to visible features and the relative position of visible area in the Roi. Weights Learner in the figure follows the Eqn. 9 and learns proposal weights. Loss is calculated via weighting classification loss and regression loss with proposal weights.

method to effectively learn weights for proposals. Given similar features from the same visible position of different proposals should give similar instructions for the classification and regression, we consider proposals with similar visible area locations as a cluster and learn weights for all of the samples within the cluster to decorrelate their ROI features. We present our method in detail as follows.

3.3.1 Clustering

We first cluster the proposals by their bounding boxes, ROI features, and visible information with a clustering function $g : \mathcal{B} \times \mathcal{Z}^{\text{Roi}} \times \{0, 1\}^{H^{\text{Roi}} \times W^{\text{Roi}}} \rightarrow [K]$. The cluster of a proposal is given by $G_{ij} \triangleq g(B_{ij}^{\text{pro}}, Z_{ij}^{\text{Roi}}, V_{ij})$. Here $V_{ij} \in \{0, 1\}^{H^{\text{Roi}} \times W^{\text{Roi}}}$ denotes the visible regions of the proposal B_{ij}^{pro} and $(V_{ij})_{hw} \in \{0, 1\}$ indicates whether the region in B_{ij}^{pro} with coordinates (h, w) is visible. For datasets without the annotation of visible areas, $V_{ij} \equiv 1^{H^{\text{Roi}} \times W^{\text{Roi}}}$.

We use k-means clustering [52] to learn the clustering function g . Let N_k^c denotes the number of proposals in cluster k , i.e., $N_k^c = \sum_{i=1}^N \sum_{j=1}^{N_{\text{pro}}} \mathbb{I}[G_{ij} = k]$.

3.3.2 RFF-based decorrelation

We propose to decorrelate ROI features after an extra spatial pooling with random fourier features (RFF) [62].

Spatial pooling In each group, we simply adopt spatial pooling to reduce the feature dimension given that no spatial difference remains after clustering. Specifically, we squeeze spatial dimensions of given ROI features in visible areas with spatial pooling function $h_{\text{SP}} : \mathcal{Z}^{\text{Roi}} \rightarrow \mathbb{R}^{C^{\text{Roi}}}$, which can be written as

$$Z_{ij}^{\text{SP}} = h_{\text{SP}}(Z_{ij}^{\text{Roi}}) = \frac{1}{N_{ij}^{\text{vis}}} \sum_{h=1}^{H^{\text{Roi}}} \sum_{w=1}^{W^{\text{Roi}}} (V_{ij})_{hw} (Z_{ij}^{\text{Roi}})_{hw}. \quad (1)$$

Here $(Z_{ij}^{\text{Roi}})_{hw}$ is a C^{Roi} -dimensional vector which represents a bin in Z_{ij}^{Roi} with coordinates (h, w) . $(N_{ij}^{\text{vis}})_{hw}$ rep-

resents the number of visible regions in Z_{ij}^{Roi} , i.e., $N_{ij}^{\text{vis}} = \sum_{h=1}^{H^{\text{Roi}}} \sum_{w=1}^{W^{\text{Roi}}} (V_{ij})_{hw}$.

Sample reweighting To eliminate the spurious correlation between domain-related features and category discriminating features, we seek to decorrelate all the features within Z^{SP} . There are many approaches for feature decorrelation, such as Hilbert-Schmidt Independence Criterion (HSIC) [23] and independent component analysis (ICA) [22], yet the calculation of them requires noticeable computational cost which grows as the batch size of training data increases, so it is inapplicable to training deep models on large datasets. Thus we adopt Random Fourier Features (RFF) [61] to capture the non-linear relationships between variables for the feature statistically independence.

Specifically, we learn sample weights to decorrelate ROI features inside each cluster by minimizing the following loss function.

$$\mathcal{L}_{\text{decorr}}(\mathbf{w}; f_{\text{rep}}, f_{\text{RPN}}, g) \triangleq \sum_{k=1}^K \sum_{1 \leq p < q \leq C^{\text{Roi}}} \left\| \hat{\Sigma}_{pq|k;\mathbf{w}} \right\|_F^2. \quad (2)$$

The space of all possible sample weights \mathcal{W} is given by

$$\mathcal{W} = \left\{ \mathbf{w} \in \mathbb{R}_+^{N \times N_{\text{pro}}} \mid \forall k \in [K], \sum_{i=1}^N \sum_{j=1}^{N_{\text{pro}}} w_{ij} \mathbb{I}[G_{ij} = k] = N_k^c \right\}, \quad (3)$$

which is a normalization operation that constraints the sum of proposal weights for each cluster to the number of samples within. In addition, $\hat{\Sigma}_{pq|k;\mathbf{w}}$ is the partial cross-covariance matrix between the p -th and q -th dimension of the ROI feature after extra spatial pooling h_{SP} , i.e., Z_{ijp}^{SP} and Z_{ijq}^{SP} , in cluster k under sample weights \mathbf{w} , which is given by

$$\begin{aligned} \hat{\Sigma}_{pq|k;\mathbf{w}} &= \frac{1}{N_k^c - 1} \sum_{i=1}^N \sum_{j=1}^{N_{\text{pro}}} \mathbb{I}[G_{ij} = k] \cdot \\ &\quad \left(w_{ij} \mathbf{r}(Z_{ijp}^{\text{SP}}) - \bar{\mathbf{r}}_{\mathbf{w},k} \right)^T \left(w_{ij} \mathbf{s}(Z_{ijq}^{\text{SP}}) - \bar{\mathbf{s}}_{\mathbf{w},k} \right). \end{aligned} \quad (4)$$

Algorithm 1 Training procedure of RAPT

```

1: for epoch  $\leftarrow 1$  to #EPOCH do
2:   for batch  $\leftarrow 1$  to #BATCH do
3:     Use K-means to learn the clustering function  $g$  in
       the batch
4:     for epoch_decorr  $\leftarrow 1$  to #EPOCH_DECORR do
5:       Optimize sample weights  $w$  in the current batch
          as shown in Equation 2
6:     end for
7:     Learn predicting functions  $f_{\text{rep}}$ ,  $f_{\text{RPN}}$ ,  $f_{\text{pred}}$  under
       learned weights  $w$  as shown in Equation 8
8:   end for
9: end for
Output: predicting functions  $f_{\text{rep}}$ ,  $f_{\text{RPN}}$ ,  $f_{\text{pred}}$ 

```

Here

$$\begin{cases} \mathbf{r}(\cdot) = (r_1(\cdot), r_2(\cdot), \dots, r_{N_{\text{RFF}}}(\cdot)), r_l(\cdot) \in \mathcal{H}_{\text{RFF}}, \forall l, \\ \mathbf{s}(\cdot) = (s_1(\cdot), s_2(\cdot), \dots, s_{N_{\text{RFF}}}(\cdot)), s_l(\cdot) \in \mathcal{H}_{\text{RFF}}, \forall l, \end{cases} \quad (5)$$

are Random Fourier Features from the following function space

$$\mathcal{H}_{\text{RFF}} = \{h : x \rightarrow \sqrt{2} \cos(\omega x + \phi) \mid \omega \sim N(0, 1), \phi \sim \text{Uniform}(0, 2\pi)\}. \quad (6)$$

$\bar{\mathbf{r}}_{w,k}$ and $\bar{\mathbf{s}}_{w,k}$ are weighted means of the corresponding functions, i.e.,

$$\begin{cases} \bar{\mathbf{r}}_{w,k} = \frac{1}{N_k^c} \sum_{i=1}^N \sum_{j=1}^{N_{\text{pro}}} w_{ij} \mathbb{I}[G_{ij} = k] \mathbf{r}(Z_{ijp}^{\text{sp}}), \\ \bar{\mathbf{s}}_{w,k} = \frac{1}{N_k^c} \sum_{i=1}^N \sum_{j=1}^{N_{\text{pro}}} w_{ij} \mathbb{I}[G_{ij} = k] \mathbf{s}(Z_{ijq}^{\text{sp}}). \end{cases} \quad (7)$$

As a result, $\mathcal{L}_{\text{decorr}}$ in Equation 2 can effectively decorrelate features in each cluster.

3.4. Training procedure

The prediction loss for the representation function f_{rep} , region proposal network f_{RPN} , and predicting function f_{pred} under weights w is given by

$$\begin{aligned} & \mathcal{L}_{\text{pred}}(f_{\text{rep}}, f_{\text{RPN}}, f_{\text{pred}}; w) \\ & \triangleq \sum_{i=1}^N \sum_{j=1}^{N_{\text{pro}}} w_{ij} \left(\mathcal{L}_{\text{cls}}(\bar{y}_{ij}, \hat{y}_{ij}) + \mathcal{L}_{\text{reg}}(\bar{B}_{ij}, \hat{B}_{ij}) \right). \end{aligned} \quad (8)$$

Here \bar{y}_{ij} and \bar{B}_{ij} are the corresponding ground truth label and bounding box w.r.t. the output $(\hat{y}_{ij}, \hat{B}_{ij})$. $\mathcal{L}_{\text{cls}}(\cdot, \cdot)$ is a standard classification loss and we adopt the binary cross entropy loss in this RAPT. $\mathcal{L}_{\text{reg}}(\cdot, \cdot)$ measures the error between the ground truth bounding box \bar{B}_{ij} and the predicted one \hat{B}_{ij} . We adopt smooth L1 loss in practice.

Our algorithm iteratively optimize detection functions (including representation function f_{rep} , region proposal network f_{RPN} , and predicting function f_{pred}), clustering function g , and sample weights w as follows:

$$\begin{cases} f_{\text{rep}}^{(t+1)}, f_{\text{RPN}}^{(t+1)}, f_{\text{pred}}^{(t+1)} = \arg \min_{f_{\text{rep}}, f_{\text{RPN}}, f_{\text{pred}}} \mathcal{L}_{\text{pred}}(f_{\text{rep}}, f_{\text{RPN}}, f_{\text{pred}}; w^{(t)}), \\ g^{(t+1)} = \text{K-means}(K, f_{\text{rep}}, f_{\text{RPN}}), \\ w^{(t+1)} = \arg \min_{w \in \mathcal{W}} \mathcal{L}_{\text{decorr}}(w; f_{\text{rep}}^{(t+1)}, f_{\text{RPN}}^{(t+1)}, g^{(t+1)}). \end{cases} \quad (9)$$

Here $f^{(t)}$, $g^{(t)}$, $w^{(t)}$ means the functions and sample weights at time stamp $t \in [T]$. K-means($K, f_{\text{rep}}, f_{\text{RPN}}$) denotes the output function of the K-means algorithm that categorizes the features $(B_{ij}^{\text{pro}}, Z_{ij}^{\text{RoI}}, V_{ij})$ generated by f_{rep} and f_{RPN} into K clusters. Initially, $w^{(0)} = (1, 1, \dots, 1)$.

Equations listed above require to learn a weight for any possible proposals in the training data, yet in practice, only part of the proposals are observed in each batch with SGD [3] as the optimizer. As a result, we slightly change the equations to calculate loss functions in each batch. A detailed training procedure of our proposed method RAPT is shown in Algorithm 1.

4. Experiments

Traditional detectors are usually evaluated with i.i.d. data, i.e., the training and test data are from a single dataset sharing the same distribution. Most current detection datasets do not consider distribution shifts or only cluster data into two domains which are insufficient for DG evaluation. The combination of different datasets for training and test can introduce significant distribution shifts since the density of objects, image contexts, illumination and filming anchors across different datasets vary largely, especially in pedestrian detection datasets. To evaluate the robustness of pedestrian detectors under distribution shifts and explore the effectiveness of cross-dataset data augments, such as whether open-world detection datasets help detection in autonomous driving scenarios, we propose four novel evaluation settings to benchmark detectors under distribution shifts between training and test data in both general detection and pedestrian detection scenarios.

4.1. Benchmark for Object Detection in Domain Generalization

Datasets. To thoroughly evaluate current detectors under distribution shifts, we adopt 5 large-scale general detection datasets and 6 pedestrian detection datasets for extensive settings.

COCO [45] is a large-scale object detection, segmentation, and captioning dataset that contains annotations of 80 different classes. In this task. We only focus on the testing results on people (label equals 1) of the validation set.

Table 1. Results (mAP) of detectors on the classic DG setting for general object detection. All detectors are reimplemented with ResNet-50 [28] pretrained on Imagenet [14] as the backbone. The title of each column indicates the dataset models are tested on while the other datasets are used as training data. The best results of all methods are highlighted with the bold font.

| Method | BDD100k | Cityscapes | Sim10k | KITTI | Mean |
|--------------------------|--------------|--------------|--------------|--------------|--------------|
| Faster RCNN | 0.371 | 0.452 | 0.303 | 0.484 | 0.403 |
| RetinaNet | 0.414 | 0.439 | 0.279 | 0.454 | 0.397 |
| Jigen + Faster RCNN | 0.374 | 0.451 | 0.295 | 0.485 | 0.401 |
| RSC + Faster RCNN | 0.356 | 0.422 | 0.297 | 0.472 | 0.387 |
| StableNet + Faster RCNN | 0.373 | 0.440 | 0.297 | 0.486 | 0.399 |
| RAPT(ours) + Faster RCNN | 0.383 | 0.459 | 0.322 | 0.490 | 0.414 |

Table 2. Results of detectors trained on CrowdHuman and ECP, and tested on CityPersons, Caltech and WiderPedestrian. The title of each column indicates the tested subset. For details about the number of runs and fonts, see Table 1.

| Method | Training Data | CityPersons | | | | Caltech | | | | WiderPedestrian |
|---------------------|----------------|---------------|---------------|---------------|---------------|---------------|---------------|---------------|---------------|-----------------|
| | | Reasonable | Small | Heavy | All | Reasonable | Small | Heavy | All | |
| CrowdDet [11] | CrowdHuman+ECP | 0.2336 | 0.3859 | 0.5170 | 0.4841 | 0.2633 | 0.3212 | 0.6722 | 0.6621 | 0.7054 |
| IterDet [67] | CrowdHuman+ECP | 0.4766 | 0.6565 | 0.7920 | 0.7326 | 0.4456 | 0.4396 | 0.8381 | 0.7710 | 0.8112 |
| ALFNet [47] | CrowdHuman+ECP | 0.2446 | 0.3791 | 0.5408 | 0.5166 | 0.2422 | 0.3435 | 0.7067 | 0.6829 | 0.7379 |
| ACSP [81] | CrowdHuman+ECP | 0.2118 | 0.4061 | 0.5685 | 0.4872 | 0.2809 | 0.3466 | 0.6369 | 0.6765 | 0.7652 |
| Det-AdvProp [9] | CrowdHuman+ECP | 0.2576 | 0.4051 | 0.5426 | 0.5391 | 0.2799 | 0.3537 | 0.7470 | 0.6851 | 0.7426 |
| LLA [19] | CrowdHuman+ECP | 0.2610 | 0.2640 | 0.5445 | 0.4956 | 0.2394 | 0.2904 | 0.6621 | 0.6361 | 0.6765 |
| RetinaNet [44] | CrowdHuman+ECP | 0.2621 | 0.4483 | 0.5082 | 0.5096 | 0.2422 | 0.2831 | 0.6578 | 0.6492 | 0.6940 |
| Cascade RCNN [6] | CrowdHuman+ECP | 0.3455 | 0.5051 | 0.6970 | 0.5696 | 0.3400 | 0.3965 | 0.7721 | 0.7164 | 0.7604 |
| Faster RCNN [65] | CrowdHuman+ECP | 0.2211 | 0.3309 | 0.4971 | 0.4705 | 0.2165 | 0.2612 | 0.6376 | 0.6162 | 0.6852 |
| RAPT (ours) + FRCNN | CrowdHuman+ECP | 0.2170 | 0.3438 | 0.4724 | 0.4583 | 0.1900 | 0.2554 | 0.6280 | 0.6126 | 0.6533 |

Table 3. Instance density of each dataset

| Dataset | # of objects/img | # of overlaps/img |
|----------------------------|------------------|-------------------|
| COCO [45] | 9.34 | 0.015 |
| Caltech [15] | 4.92 | 0.08 |
| Citypersons [95] | 6.47 | 0.32 |
| EuroCity Persons (ECP) [4] | 11.65 | 0.63 |
| CrowdHuman [70] | 22.64 | 2.40 |
| WiderPedestrian [51] | 6.05 | 0.09 |

Table 4. Evaluation splits.

| Setting | Resonable | Small | Heavy | All |
|------------|----------------|-------------|----------------|----------------|
| Height | $[50, \infty)$ | $[50, 75]$ | $[50, \infty)$ | $[20, \infty)$ |
| Visibility | $[0.65, 1]$ | $[0.65, 1]$ | $[0.2, 0.65]$ | $[0.2, 1]$ |

BDD100k [85] is a large-scale, diverse dataset for autonomous driving and consists of 100,000 videos. It covers different weather conditions, including sunny, overcast, and rainy, as well as different times of day including daytime and nighttime.

Cityscapes [12] consists of 2975 training samples and 500 validation samples for semantic understanding of urban street scenes. The images are taken from 50 cities on daytime with totally 30 object categories.

Sim10k [35] is a synthetic dataset containing 10,000 im-

ages. It is generated based on the video game Grand Theft Auto V (GTA V) by incorporating photo-realistic computer images from a simulation engine to rapidly generate annotated data that can be used for the training of machine learning algorithms.

KITTI [20] for object detection and object orientation estimation benchmark consists of 7481 training images and 7518 test images, comprising a total of 80,256 labeled objects. All images were taken on the street by cameras on cars.

Caltech [15] consists of approximately 10 hours of 640x480 30Hz video taken from a vehicle driving through regular traffic in an urban environment. About 250,000 frames (in 137 approximately minute long segments) with a total of 350,000 bounding boxes and 2300 unique pedestrians were annotated. All experiments on Caltech are conducted under the new annotations provided by [94].

Citypersons [95] is a subset of Cityscapes [12] which only consists of person annotations and exhibits more diversity when compared with Caltech [15]. There are 2975 images for training, 500 and 1575 images for validation and testing.

EuroCity Persons (ECP) [4] is a new dataset that is recorded in 31 different cities across 12 countries in Europe. It has 40,217 images for daytime and 7118 images for nighttime (thus referred to as ECP daytime and ECP nighttime). Total annotated bounding boxes are over 200K. As

Table 5. Results of detectors trained on sparse datasets and tested on crowd ones. For details about the number of runs, meaning of column titles and fonts, see Table 2.

| Model | Training Data | CrowdHuman | | | | ECP | | | |
|------------------------|--------------------|---------------|---------------|---------------|---------------|---------------|---------------|---------------|---------------|
| | | Reasonable | Small | Heavy | All | Reasonable | Small | Heavy | All |
| IterDet | City+Caltech+Wider | 0.6135 | 0.4728 | 0.9126 | 0.8172 | 0.3724 | 0.5431 | 0.8101 | 0.6384 |
| ALFNet | City+Caltech+Wider | 0.5252 | 0.4473 | 0.8912 | 0.7917 | 0.2453 | 0.3846 | 0.7077 | 0.5755 |
| ACSP | City+Caltech+Wider | 0.5876 | 0.4278 | 0.8842 | 0.7981 | 0.2518 | 0.3765 | 0.7483 | 0.5782 |
| Det-AdvProp | City+Caltech+Wider | 0.5236 | 0.4597 | 0.8911 | 0.7573 | 0.2305 | 0.3293 | 0.6719 | 0.5630 |
| LLA | City+Caltech+Wider | 0.5280 | 0.4315 | 0.8900 | 0.7793 | 0.2342 | 0.3533 | 0.7017 | 0.5340 |
| RetinaNet | City+Caltech+Wider | 0.5884 | 0.4683 | 0.8770 | 0.8175 | 0.2619 | 0.3978 | 0.6878 | 0.5680 |
| Cascade RCNN | City+Caltech+Wider | 0.6631 | 0.5164 | 0.9108 | 0.8190 | 0.3781 | 0.4610 | 0.8561 | 0.6370 |
| Faster RCNN | City+Caltech+Wider | 0.5080 | 0.4195 | 0.8635 | 0.7600 | 0.2493 | 0.3703 | 0.7182 | 0.5549 |
| RAPT (ours) + FRCNN | City+Caltech+Wider | 0.4970 | 0.3938 | 0.8748 | 0.7480 | 0.1987 | 0.2796 | 0.6673 | 0.5238 |
| CrowdDet | City+Caltech+Wider | 0.4907 | 0.4058 | 0.8642 | 0.7443 | 0.2106 | 0.3008 | 0.6778 | 0.5031 |
| RAPT (ours) + CrowdDet | City+Caltech+Wider | 0.4715 | 0.3980 | 0.8698 | 0.7305 | 0.1998 | 0.2650 | 0.6604 | 0.4927 |

Table 6. Results of detectors trained on open-world datasets and tested on autonomous driving ones. For details about the number of runs, meaning of column titles and fonts, see Table 2.

| Model | Training | ECP | | | | Caltech | | | | CityPersons | | | |
|---------------------|----------|---------------|---------------|---------------|---------------|---------------|---------------|---------------|---------------|---------------|---------------|---------------|---------------|
| | | Reasonable | Small | Heavy | All | Reasonable | Small | Heavy | All | Reasonable | Small | Heavy | All |
| CrowdDet | C+W | 0.2293 | 0.3802 | 0.7276 | 0.5364 | 0.2292 | 0.2786 | 0.6293 | 0.6299 | 0.2984 | 0.4940 | 0.6493 | 0.5449 |
| IterDet | C+W | 0.4057 | 0.6111 | 0.8268 | 0.6614 | 0.2727 | 0.3271 | 0.7054 | 0.6895 | 0.4051 | 0.5984 | 0.7650 | 0.6272 |
| ALFNet | C+W | 0.2569 | 0.4146 | 0.7285 | 0.5636 | 0.2552 | 0.2896 | 0.6418 | 0.6489 | 0.3036 | 0.4662 | 0.6317 | 0.5559 |
| ACSP | C+W | 0.2780 | 0.4219 | 0.7644 | 0.5808 | 0.2225 | 0.2581 | 0.6451 | 0.6404 | 0.2967 | 0.5584 | 0.6962 | 0.5669 |
| LLA | C+W | 0.2352 | 0.3761 | 0.7451 | 0.5428 | 0.2155 | 0.2628 | 0.6357 | 0.6235 | 0.3190 | 0.4557 | 0.6733 | 0.5632 |
| RetinaNet | C+W | 0.2576 | 0.4079 | 0.7072 | 0.5659 | 0.2156 | 0.2512 | 0.6237 | 0.6312 | 0.3169 | 0.5114 | 0.6250 | 0.5654 |
| Cascade RCNN | C+W | 0.3390 | 0.4632 | 0.8298 | 0.6140 | 0.2734 | 0.3129 | 0.6849 | 0.6716 | 0.3608 | 0.5243 | 0.7518 | 0.5933 |
| Faster RCNN | C+W | 0.2162 | 0.3499 | 0.7035 | 0.5239 | 0.2337 | 0.2826 | 0.6206 | 0.6297 | 0.2912 | 0.4679 | 0.6139 | 0.5364 |
| RAPT (ours) + FRCNN | C+W | 0.1982 | 0.3209 | 0.7144 | 0.4993 | 0.2282 | 0.2635 | 0.6122 | 0.6134 | 0.2942 | 0.4414 | 0.5849 | 0.5193 |

mentioned in ECP, for the sake of comparison with other approaches, all experiments and comparisons are made on the daytime ECP. ECP surpasses Caltech and Citypersons a lot in terms of diversity and difficulty.

CrowdHuman [70] is a benchmark dataset to better evaluate detectors in crowd scenarios which contain 15,000, 4,370, and 5,000 images for training, validation, and test, respectively. We test the results on the validation dataset under the same settings for a fair comparison.

WiderPedestrian [51] is a non-traffic related recent benchmark dataset that contains 43,378 and 5,000 images for training and validation, we only compare the mean miss rate on the validation set due to the lack of visible bounding box annotations.

Benchmark. For general object detection, we consider the classic evaluation method in DG, leave-one-out evaluation [39]. Specifically, we consider 4 datasets, namely BDD100K, Cityscapes, Sim10K and KITTI as 4 domains, and train detectors on three of them while test on the last for each run. For pedestrian detection scenarios, we consider three kinds of simple yet common distribution shifts in real pedestrian detection applications and split these datasets into subgroups, resulting in three corresponding evaluation

settings, namely density shift, context shift, and random shift. For each setting, we divide datasets into training split and testing split following the corresponding rule. For each dataset in the training split, we train detectors with its training subset, while for each dataset in the testing split, we test detectors with its testing or validation subset. We train each model 30K iterations for each epoch while the same amount of data are sampled from each training dataset to restrict the impact of difference of dataset sizes.

We evaluate detectors with the widely accepted criterion, mean Average Precision (mAP) and MR^{-2} (i.e., log average miss rate over False Positive Per Image (FPPI) over range $[10^{-2}, 10^0]$). Given occlusion is a key factor affecting the performance, we report different occlusion levels as shown in Table 4, following [25]. Visible part is not labeled in WiderPedestrian, thus we report the overall MR^{-2} . More results are in Appendix.

Training details. We adopt ResNet-50 as the backbone of all methods. All of the methods are trained for 20 epochs and 30K iteration each epoch. We follow the settings of hyperparameters presented in corresponding original papers, respectively. The initial learning rate is set to 0.02 and decayed by a factor of 10 after the 14th epoch and 18th epoch.

Table 7. Results of detectors trained on autonomous driving datasets and tested on open-world ones. For details about the number of runs, meaning of column titles and fonts, see Table 2.

| Model | Training Data | CrowdHuman | | | | WiderPedestrian |
|--------------|------------------|---------------|---------------|---------------|---------------|-----------------|
| | | Reasonable | Small | Heavy | All | |
| CrowdDet | ECP+Caltech+City | 0.6757 | 0.6178 | 0.9251 | 0.8329 | 0.8084 |
| IterDet | ECP+Caltech+City | 0.9217 | 0.7482 | 0.9683 | 0.9541 | 0.9196 |
| ALFNet | ECP+Caltech+City | 0.8453 | 0.6719 | 0.9295 | 0.9012 | 0.8185 |
| ACSP | ECP+Caltech+City | 0.8934 | 0.6645 | 0.9633 | 0.9472 | 0.8063 |
| LLA | ECP+Caltech+City | 0.6527 | 0.5800 | 0.9141 | 0.8232 | 0.8191 |
| RetinaNet | ECP+Caltech+City | 0.6868 | 0.6569 | 0.9247 | 0.8523 | 0.8030 |
| Cascade RCNN | ECP+Caltech+City | 0.8347 | 0.7566 | 0.9681 | 0.9113 | 0.8823 |
| Faster RCNN | ECP+Caltech+City | 0.6451 | 0.5776 | 0.9122 | 0.8164 | 0.8003 |
| RAPT (ours) | ECP+Caltech+City | 0.6476 | 0.5619 | 0.9013 | 0.8078 | 0.7852 |

Table 8. Results of detectors evaluated under random distribution shifts. For details about the number of runs, meaning of column titles and fonts, see Table 2.

| Model | Training Data | CrowdHuman | | | | Caltech | | | | WiderPedestrian | COCO |
|-------------------|---------------|---------------|---------------|---------------|---------------|---------------|---------------|---------------|---------------|-----------------|---------------|
| | | Reasonable | Small | Heavy | All | Reasonable | Small | Heavy | All | | |
| CrowdDet | ECP+City | 0.5813 | 0.4494 | 0.8721 | 0.7677 | 0.3452 | 0.4114 | 0.7293 | 0.7112 | 0.7375 | 0.7869 |
| IterDet | ECP+City | 0.8884 | 0.7277 | 0.9477 | 0.9463 | 0.3852 | 0.4554 | 0.7872 | 0.7742 | 0.8876 | 0.9774 |
| ALFNet | ECP+City | 0.6005 | 0.5129 | 0.8715 | 0.8063 | 0.3595 | 0.4278 | 0.8219 | 0.7452 | 0.8251 | 0.8051 |
| LLA | ECP+City | 0.5884 | 0.4660 | 0.8869 | 0.7841 | 0.2849 | 0.3610 | 0.7304 | 0.6855 | 0.7516 | 0.7707 |
| RetinaNet | ECP+City | 0.5665 | 0.4521 | 0.8567 | 0.7866 | 0.3281 | 0.4027 | 0.7428 | 0.7135 | 0.7377 | 0.7521 |
| Faster RCNN | ECP+City | 0.5668 | 0.4544 | 0.8513 | 0.7643 | 0.3330 | 0.4082 | 0.7196 | 0.7109 | 0.7332 | 0.7844 |
| RAPT (ours)+FRCNN | ECP+City | 0.5639 | 0.4100 | 0.8606 | 0.7526 | 0.3051 | 0.3587 | 0.6952 | 0.6937 | 0.7251 | 0.7742 |

We train all the methods on 8 GPUs and set the minibatch size to 16. The short edge of input images is resized to 1024 and the long edge is smaller than 1792. To reduce the impact of imbalance of data amount, we ensure that approximately the same number of images are sampled from each training datasets for each epoch.

4.2. Classic DG Evaluation in General Object Detection

We consider the classic DG evaluation method to evaluate detectors' generalization ability, where one dataset is selected for test and the others for training for each run. Note that for DG evaluation, knowledge of test distribution is completely inaccessible in the training phase, so that current detection methods designed for domain adaptation (DA) [17, 24, 34, 55] are not applicable. Moreover, most current DG methods are designed for image classification and the adaptation of them in the object detection task is nontrivial [41, 60, 75].

Other than Faster R-CNN and RetinaNet, we select and reimplement the following model-agnostic DG methods as baselines. **Jigen** [8]. Jigen is a representative representation enhancement based method for DG without requirement of any extra annotations. We introduce an extra jigsaw classifier to Faster R-CNN and minimize the image-level jigsaw loss as suggested in the paper. **RSC**. [32] RSC is a dropout

based DG method that iteratively discards the dominant features activated on the training data. **StableNet** [98]. StableNet proposed to improve the generalization ability under distribution shifts via sample reweighting. We directly calculate RFF of image representations and adopt the image-wise reweighting in a Faster R-CNN model.

These methods are easy to be assembled with object detection since they are not strongly coupled with the classification task and do not require domain labels. The results are shown in Table 1. The direct combinations of current DG methods and Faster R-CNN fail to achieve significant improvement, which may be caused by the two-stage optimization in Faster R-CNN and the small batch size (compared with the classification task, the batch size in object detection is considerably small). This further indicates that although the field of DGOB is of critical importance for real-world applications, it lacks competitive specially designed methods.

4.3. Density Shift

We investigate how the density shift between training and testing data affects current pedestrian detectors and the proposed method. Since pedestrian detection is widely used in many real-world applications where pedestrians can be excessively crowded (e.g., shopping malls, airports, and train stations) or quite sparse (e.g., streets and schoolyards),

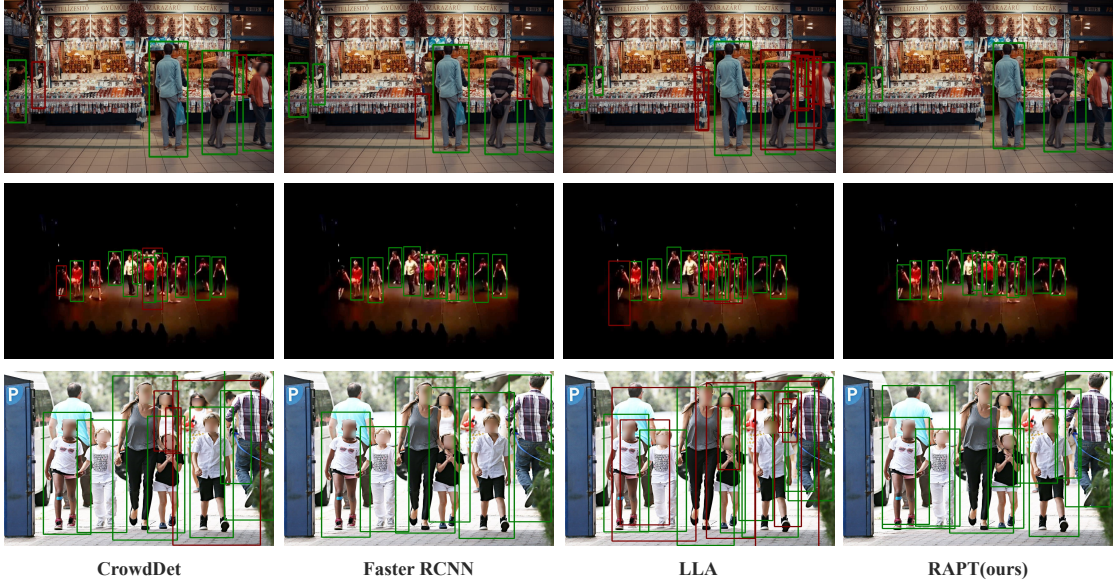


Figure 3. Visualization of bounding boxes detected by RAPT, CrowdDet, LLA and Faster RCNN. RAPT yields less wrong detected bounding boxes (marked with red anchors) compared with CrowdDet and LLA, and more accurate bounding boxes than Faster RCNN.

the generalization ability of detectors across people density is of great importance.

Several previous works [11, 19, 25] have discussed the definition and impact of the instance density of pedestrian detection datasets under i.i.d. settings, yet none of them consider the distribution shift caused by the diversity of different datasets in instance density. We summarize the instance density of pedestrian detection datasets in Table 3. We set the threshold of objects per image to 10 and cluster these datasets into dense ones, namely CrowdHuman, ECP, and sparse ones, namely WiderPedestrian, Caltech, and Citypersons. We first investigate the generalization ability of models trained on dense datasets and tested on sparse datasets.

Results of detectors trained on dense scenes and tested on sparse scenes are shown in Table 2. Surprisingly, we find that detectors specifically designed for pedestrian detection show worse performance compared with general object detectors. Even pedestrian detectors especially proposed for crowd scenarios such as CrowdDet [11] and IterDet [67] fail to outperform general detectors such as Faster RCNN [65], indicating that though these methods show outstanding performance when tested in crowd scenarios, they fail to learn invariant features from data with different people densities. The proposed RAPT, on the contrary, achieves the best performance on almost all of the sub-settings.

Results of detectors trained on sparse scenes and tested on dense ones are shown in Table 5. Compared with Faster RCNN and RetinaNet [44], dense pedestrian detectors show superior performance. As a plug-in module, RAPT can be combined with any proposal-based detectors to improve

their generalization ability under distribution shifts. We can easily introduce RAPT to CrowdDet via learning proposal weights for multiple proposals generated by CrowdDet and reweighting valid proposals to calculate final losses. We present results of RAPT with Faster RCNN and CrowdDet as the base model, respectively in Table 5. RAPT further improves the performance of CrowdDet under dense testing scenarios.

4.4. Context Shift

Contexts of popular pedestrian detection benchmarks can be split into street scenarios and open-world scenarios. Datasets with street contexts, such as CityPersons, Caltech, and EuroCity Persons, can also be considered as autonomous driving datasets, while others, such as CrowdHuman and WiderPedestrian, are non-traffic related datasets.

Investigating generalization ability from non-traffic-related data to autonomous driving data is of critical importance, given that pedestrian detection for autonomous driving is required to generate accurate predictions under any possible environments, which may exceed the coverage of training distribution. Moreover, data from open-world scenarios are more heterogeneous and easy to collect so that they can provide significant diversity of human features, such as various postures and occlusion situations. Thus the robustness of the model when adopted in unknown autonomous driving scenarios can be largely improved via non-traffic-related data.

We first train our proposed method and state-of-the-art pedestrian detectors on non-traffic-related datasets before evaluating them on datasets with street scenarios context.

Results are shown in Table 6. When testing on ECP, general detectors achieve better performance compared with pedestrian detectors, while ACSP [81] shows advanced accuracy on *reasonable* and *small* sets of CityPersons. With raw Faster RCNN as the base model, RAPT shows the best performance on most of the settings, which indicates that the robustness of detectors for autonomous driving can be strengthened by RAPT with non-traffic data. Then we train detectors on traffic-related datasets and test them on the remaining ones and show the results in Table 7. RAPT consistently outperforms its state-of-the-art counterparts, showing clear improvements in generalization ability.

4.5. Random Shift

We consider the random distribution shifts between training and testing data. Pedestrian detectors can encounter random or uncertain shifts other than pre-set ones such as *density shift* and *context shift*. We randomly select several datasets for training and others for evaluation to generate random distribution shifts. Here we present the results of training with ECP and CityPersons, testing with CrowdHuman, Caltech, and WiderPedestrian in Table 8. More experimental results under other splits of datasets are shown in Appendix.

As shown in Table 8, RAPT outperforms other methods under random distribution shifts. Visualizations of bounding boxes detected by RAPT, CrowdDet, and Faster RCNN are shown in Figure 3. RAPT generates more accurate bounding boxes and fewer wrong bounding boxes, indicating a clear improvement of generalization ability under random distribution shifts.

5. Conclusions

In this paper, to investigate the impact of distribution shifts, we proposed three novel cross-dataset evaluation settings for pedestrian detectors. Then we proposed a novel method named RAPT, which can eliminate the statistical correlation between relevant and irrelevant features via learning proposal samples with ROI features, to improve the generalization of detection models under distribution shifts. Extensive experiments across several datasets and settings proved the effectiveness of our proposed method.

References

- [1] Martin Arjovsky, Léon Bottou, Ishaan Gulrajani, and David Lopez-Paz. Invariant risk minimization. *arXiv preprint arXiv:1907.02893*, 2019. [2](#)
- [2] Alexey Bochkovskiy, Chien-Yao Wang, and Hong-Yuan Mark Liao. Yolov4: Optimal speed and accuracy of object detection. *arXiv preprint arXiv:2004.10934*, 2020. [2](#)
- [3] Léon Bottou and Olivier Bousquet. 13 the tradeoffs of large-scale learning. *Optimization for machine learning*, page 351, 2011. [5](#)
- [4] Markus Braun, Sebastian Krebs, Fabian Flohr, and Dariu M Gavrila. Eurocity persons: A novel benchmark for person detection in traffic scenes. *IEEE transactions on pattern analysis and machine intelligence*, 41(8):1844–1861, 2019. [1, 6](#)
- [5] Qi Cai, Yingwei Pan, Chong-Wah Ngo, Xinmei Tian, Lingyu Duan, and Ting Yao. Exploring object relation in mean teacher for cross-domain detection. In *Proceedings of the IEEE/CVF Conference on Computer Vision and Pattern Recognition*, pages 11457–11466, 2019. [3](#)
- [6] Zhaowei Cai and Nuno Vasconcelos. Cascade r-cnn: High quality object detection and instance segmentation. *IEEE Transactions on Pattern Analysis and Machine Intelligence*, 2019. [6, 15](#)
- [7] Fabio M Carlucci, Antonio D’Innocente, Silvia Bucci, Barbara Caputo, and Tatiana Tommasi. Domain generalization by solving jigsaw puzzles. In *Proceedings of the IEEE/CVF Conference on Computer Vision and Pattern Recognition*, pages 2229–2238, 2019. [3](#)
- [8] Fabio Maria Carlucci, Antonio D’Innocente, Silvia Bucci, Barbara Caputo, and Tatiana Tommasi. Domain generalization by solving jigsaw puzzles. *2019 IEEE/CVF Conference on Computer Vision and Pattern Recognition (CVPR)*, pages 2224–2233, 2019. [8](#)
- [9] Xiangning Chen, Cihang Xie, Mingxing Tan, Li Zhang, Cho-Jui Hsieh, and Boqing Gong. Robust and accurate object detection via adversarial learning. In *Proceedings of the IEEE/CVF Conference on Computer Vision and Pattern Recognition*, pages 16622–16631, 2021. [1, 6, 15](#)
- [10] Yuhua Chen, Wen Li, Christos Sakaridis, Dengxin Dai, and Luc Van Gool. Domain adaptive faster r-cnn for object detection in the wild. In *Proceedings of the IEEE conference on computer vision and pattern recognition*, pages 3339–3348, 2018. [3](#)
- [11] Xuangeng Chu, Anlin Zheng, Xiangyu Zhang, and Jian Sun. Detection in crowded scenes: One proposal, multiple predictions. In *Proceedings of the IEEE/CVF Conference on Computer Vision and Pattern Recognition*, pages 12214–12223, 2020. [2, 6, 9, 15](#)
- [12] Marius Cordts, Mohamed Omran, Sebastian Ramos, Timo Rehfeld, Markus Enzweiler, Rodrigo Benenson, Uwe Franke, Stefan Roth, and Bernt Schiele. The cityscapes dataset for semantic urban scene understanding. In *Proc. of the IEEE Conference on Computer Vision and Pattern Recognition (CVPR)*, 2016. [6](#)
- [13] Jifeng Dai, Haozhi Qi, Yuwen Xiong, Yi Li, Guodong Zhang, Han Hu, and Yichen Wei. Deformable convolutional networks. In *Proceedings of the IEEE international conference on computer vision*, pages 764–773, 2017. [2, 3](#)
- [14] Jia Deng, Wei Dong, Richard Socher, Li-Jia Li, Kai Li, and Li Fei-Fei. Imagenet: A large-scale hierarchical image database. In *2009 IEEE conference on computer vision and pattern recognition*, pages 248–255. Ieee, 2009. [6, 15](#)
- [15] Piotr Dollar, Christian Wojek, Bernt Schiele, and Pietro Perona. Pedestrian detection: An evaluation of the state of the art. *IEEE transactions on pattern analysis and machine intelligence*, 34(4):743–761, 2011. [1, 6](#)

- [16] Kaiwen Duan, Song Bai, Lingxi Xie, Honggang Qi, Qingming Huang, and Qi Tian. Centernet: Keypoint triplets for object detection. In *Proceedings of the IEEE/CVF international conference on computer vision*, pages 6569–6578, 2019. 2
- [17] K. Fujii and K. Kawamoto. Generative and self-supervised domain adaptation for one-stage object detection. *Array*, 2021. 8
- [18] Yaroslav Ganin, Evgeniya Ustinova, Hana Ajakan, Pascal Germain, Hugo Larochelle, François Laviolette, Mario Marchand, and Victor Lempitsky. Domain-adversarial training of neural networks. *The journal of machine learning research*, 17(1):2096–2030, 2016. 2, 3
- [19] Zheng Ge, Jianfeng Wang, Xin Huang, Songtao Liu, and Osamu Yoshie. Lla: Loss-aware label assignment for dense pedestrian detection. *arXiv preprint arXiv:2101.04307*, 2021. 6, 9, 15
- [20] Andreas Geiger, Philip Lenz, and Raquel Urtasun. Are we ready for autonomous driving? the kitti vision benchmark suite. In *Conference on Computer Vision and Pattern Recognition (CVPR)*, 2012. 6
- [21] Ross Girshick. Fast r-cnn. In *Proceedings of the IEEE international conference on computer vision*, pages 1440–1448, 2015. 3
- [22] Arthur Gretton, Olivier Bousquet, Alex Smola, and Bernhard Schölkopf. Measuring statistical dependence with hilbert-schmidt norms. In *International conference on algorithmic learning theory*, pages 63–77. Springer, 2005. 4
- [23] Arthur Gretton, Kenji Fukumizu, Choon H Teo, Le Song, Bernhard Schölkopf, and Alex J Smola. A kernel statistical test of independence. In *Advances in neural information processing systems*, pages 585–592, 2008. 4
- [24] Dayan Guan, Jiaxing Huang, Aoran Xiao, Shijian Lu, and Yanpeng Cao. Uncertainty-aware unsupervised domain adaptation in object detection. *ArXiv*, abs/2103.00236, 2021. 1, 3, 8
- [25] Irtiza Hasan, Shengcui Liao, Jinpeng Li, Saad Ullah Akram, and Ling Shao. Generalizable pedestrian detection: The elephant in the room. In *Proceedings of the IEEE/CVF Conference on Computer Vision and Pattern Recognition*, pages 11328–11337, 2021. 1, 2, 7, 9, 15
- [26] Amal Hbaieb, Jihene Rezgui, and Lamia Chaari. Pedestrian detection for autonomous driving within cooperative communication system. In *2019 IEEE Wireless Communications and Networking Conference (WCNC)*, pages 1–6. IEEE, 2019. 1
- [27] Kaiming He, Georgia Gkioxari, Piotr Dollár, and Ross Girshick. Mask r-cnn. In *Proceedings of the IEEE international conference on computer vision*, pages 2961–2969, 2017. 3
- [28] Kaiming He, Xiangyu Zhang, Shaoqing Ren, and Jian Sun. Deep residual learning for image recognition. In *Proceedings of the IEEE conference on computer vision and pattern recognition*, pages 770–778, 2016. 6, 15
- [29] Yue He, Zheyen Shen, and Peng Cui. Towards non-iid image classification: A dataset and baselines. *Pattern Recognition*, 110:107383, 2021. 2
- [30] Jan Hosang, Mohamed Omran, Rodrigo Benenson, and Bernt Schiele. Taking a deeper look at pedestrians. In *Proceedings of the IEEE conference on computer vision and pattern recognition*, pages 4073–4082, 2015. 2
- [31] Han-Kai Hsu, Chun-Han Yao, Yi-Hsuan Tsai, Wei-Chih Hung, Hung-Yu Tseng, Maneesh Singh, and Ming-Hsuan Yang. Progressive domain adaptation for object detection. In *Proceedings of the IEEE/CVF winter conference on applications of computer vision*, pages 749–757, 2020. 1
- [32] Zeyi Huang, Haohan Wang, Eric P. Xing, and Dong Huang. Self-challenging improves cross-domain generalization. In *ECCV*, 2020. 8
- [33] Naoto Inoue, Ryosuke Furuta, Toshihiko Yamasaki, and Kiyoharu Aizawa. Cross-domain weakly-supervised object detection through progressive domain adaptation. In *Proceedings of the IEEE conference on computer vision and pattern recognition*, pages 5001–5009, 2018. 1
- [34] N. Inoue, R. Furuta, T. Yamasaki, and K. Aizawa. Cross-domain weakly-supervised object detection through progressive domain adaptation. *IEEE*, 2018. 8
- [35] Matthew Johnson-Roberson, Charles Barto, Rounak Mehta, Sharath Nittur Sridhar, Karl Rosaen, and Ram Vasudevan. Driving in the matrix: Can virtual worlds replace human-generated annotations for real world tasks? *arXiv preprint arXiv:1610.01983*, 2016. 6
- [36] Kun Kuang, Ruoxuan Xiong, Peng Cui, Susan Athey, and Bo Li. Stable prediction with model misspecification and agnostic distribution shift. In *Proceedings of the AAAI Conference on Artificial Intelligence*, volume 34, pages 4485–4492, 2020. 2
- [37] Brenden M Lake, Tomer D Ullman, Joshua B Tenenbaum, and Samuel J Gershman. Building machines that learn and think like people. *Behavioral and brain sciences*, 40, 2017. 2
- [38] Hei Law and Jia Deng. Cornernet: Detecting objects as paired keypoints. In *Proceedings of the European conference on computer vision (ECCV)*, pages 734–750, 2018. 2
- [39] Da Li, Yongxin Yang, Yi-Zhe Song, and Timothy M Hospedales. Deeper, broader and artier domain generalization. In *Proceedings of the IEEE international conference on computer vision*, pages 5542–5550, 2017. 2, 7
- [40] Da Li, Yongxin Yang, Yi-Zhe Song, and Timothy M Hospedales. Learning to generalize: Meta-learning for domain generalization. In *Thirty-Second AAAI Conference on Artificial Intelligence*, 2018. 3
- [41] Da Li, Yongxin Yang, Yi-Zhe Song, and Timothy M. Hospedales. Learning to generalize: Meta-learning for domain generalization. *ArXiv*, abs/1710.03463, 2018. 8
- [42] Haoliang Li, Sinno Jialin Pan, Shiqi Wang, and Alex C Kot. Domain generalization with adversarial feature learning. In *Proceedings of the IEEE Conference on Computer Vision and Pattern Recognition*, pages 5400–5409, 2018. 2, 3
- [43] Tsung-Yi Lin, Piotr Doll’ar, Ross Girshick, Kaiming He, Bharath Hariharan, and Serge Belongie. Feature pyramid networks for object detection. In *Proceedings of the IEEE conference on computer vision and pattern recognition*, pages 2117–2125, 2017. 2

- [44] Tsung-Yi Lin, Priya Goyal, Ross Girshick, Kaiming He, and Piotr Dollár. Focal loss for dense object detection. In *Proceedings of the IEEE international conference on computer vision*, pages 2980–2988, 2017. [2](#), [3](#), [6](#), [9](#), [15](#)
- [45] Tsung-Yi Lin, Michael Maire, Serge Belongie, James Hays, Pietro Perona, Deva Ramanan, Piotr Dollár, and C Lawrence Zitnick. Microsoft coco: Common objects in context. In *European conference on computer vision*, pages 740–755. Springer, 2014. [5](#), [6](#)
- [46] Wei Liu, Dragomir Anguelov, Dumitru Erhan, Christian Szegedy, Scott Reed, Cheng-Yang Fu, and Alexander C Berg. Ssd: Single shot multibox detector. In *European conference on computer vision*, pages 21–37. Springer, 2016. [2](#)
- [47] Wei Liu, Shengcai Liao, Weidong Hu, Xuezhi Liang, and Xiao Chen. Learning efficient single-stage pedestrian detectors by asymptotic localization fitting. In *Proceedings of the European Conference on Computer Vision (ECCV)*, pages 618–634, 2018. [2](#), [6](#)
- [48] Yang Liu, Peng Sun, Nickolas Wergeles, and Yi Shang. A survey and performance evaluation of deep learning methods for small object detection. *Expert Systems with Applications*, 172:114602, 2021. [1](#)
- [49] Mingsheng Long, Yue Cao, Jianmin Wang, and Michael Jordan. Learning transferable features with deep adaptation networks. In *International conference on machine learning*, pages 97–105. PMLR, 2015. [3](#)
- [50] David Lopez-Paz, Robert Nishihara, Soumith Chintala, Bernhard Schölkopf, and Léon Bottou. Discovering causal signals in images. In *Proceedings of the IEEE Conference on Computer Vision and Pattern Recognition*, pages 6979–6987, 2017. [2](#)
- [51] Chen Change Loy, Dahua Lin, Wanli Ouyang, Yuanjun Xiong, Shuo Yang, Qingqiu Huang, Dongzhan Zhou, Wei Xia, Quanquan Li, Ping Luo, et al. Wider face and pedestrian challenge 2018: Methods and results. *arXiv preprint arXiv:1902.06854*, 2019. [6](#), [7](#)
- [52] James MacQueen et al. Some methods for classification and analysis of multivariate observations. In *Proceedings of the fifth Berkeley symposium on mathematical statistics and probability*, volume 1, pages 281–297. Oakland, CA, USA, 1967. [4](#)
- [53] Gary Marcus. Deep learning: A critical appraisal. *arXiv preprint arXiv:1801.00631*, 2018. [2](#)
- [54] Krikamol Muandet, David Balduzzi, and Bernhard Schölkopf. Domain generalization via invariant feature representation. In *International Conference on Machine Learning*, pages 10–18. PMLR, 2013. [2](#), [3](#)
- [55] Farzeen Munir, Shoaib Azam, and Moongu Jeon. Sstn: Self-supervised domain adaptation thermal object detection for autonomous driving. *2021 IEEE/RSJ International Conference on Intelligent Robots and Systems (IROS)*, pages 206–213, 2021. [8](#)
- [56] Yanwei Pang, Jin Xie, Muhammad Haris Khan, Rao Muhammad Anwer, Fahad Shahbaz Khan, and Ling Shao. Mask-guided attention network for occluded pedestrian detection. In *Proceedings of the IEEE/CVF International Conference on Computer Vision*, pages 4967–4975, 2019. [2](#)
- [57] Xingchao Peng, Qinxun Bai, Xide Xia, Zijun Huang, Kate Saenko, and Bo Wang. Moment matching for multi-source domain adaptation. In *Proceedings of the IEEE/CVF International Conference on Computer Vision*, pages 1406–1415, 2019. [2](#)
- [58] Xue Bin Peng, Marcin Andrychowicz, Wojciech Zaremba, and Pieter Abbeel. Sim-to-real transfer of robotic control with dynamics randomization. In *2018 IEEE international conference on robotics and automation (ICRA)*, pages 3803–3810. IEEE, 2018. [3](#)
- [59] Fengchun Qiao, Long Zhao, and Xi Peng. Learning to learn single domain generalization. In *Proceedings of the IEEE/CVF Conference on Computer Vision and Pattern Recognition*, pages 12556–12565, 2020. [3](#)
- [60] Fengchun Qiao, Long Zhao, and Xi Peng. Learning to learn single domain generalization. *2020 IEEE/CVF Conference on Computer Vision and Pattern Recognition (CVPR)*, pages 12553–12562, 2020. [8](#)
- [61] Ali Rahimi and Benjamin Recht. Random features for large-scale kernel machines. In *Advances in neural information processing systems*, pages 1177–1184, 2008. [4](#)
- [62] Ali Rahimi, Benjamin Recht, et al. Random features for large-scale kernel machines. In *NIPS*, volume 3, page 5. Citeseer, 2007. [4](#)
- [63] Joseph Redmon, Santosh Divvala, Ross Girshick, and Ali Farhadi. You only look once: Unified, real-time object detection. In *Proceedings of the IEEE conference on computer vision and pattern recognition*, pages 779–788, 2016. [2](#)
- [64] Joseph Redmon and Ali Farhadi. Yolov3: An incremental improvement. *arXiv preprint arXiv:1804.02767*, 2018. [2](#)
- [65] Shaoqing Ren, Kaiming He, Ross Girshick, and Jian Sun. Faster r-cnn: Towards real-time object detection with region proposal networks. *Advances in neural information processing systems*, 28:91–99, 2015. [2](#), [6](#), [9](#), [15](#)
- [66] Adrian Lopez Rodriguez and Krystian Mikolajczyk. Domain adaptation for object detection via style consistency. *arXiv preprint arXiv:1911.10033*, 2019. [3](#)
- [67] Danila Rukhovich, Konstantin Sofiiuk, Danil Galeev, Olga Barinova, and Anton Konushin. Iterdet: Iterative scheme for object detection in crowded environments. In *Joint IAPR International Workshops on Statistical Techniques in Pattern Recognition (SPR) and Structural and Syntactic Pattern Recognition (SSPR)*, pages 344–354. Springer, 2021. [2](#), [6](#), [9](#), [15](#)
- [68] Kuniaki Saito, Yoshitaka Ushiku, Tatsuya Harada, and Kate Saenko. Strong-weak distribution alignment for adaptive object detection. In *Proceedings of the IEEE/CVF Conference on Computer Vision and Pattern Recognition*, pages 6956–6965, 2019. [3](#)
- [69] Shiv Shankar, Vihari Piratla, Soumen Chakrabarti, Siddhartha Chaudhuri, Preethi Jyothi, and Sunita Sarawagi. Generalizing across domains via cross-gradient training. In *International Conference on Learning Representations*, 2018. [2](#), [3](#)
- [70] Shuai Shao, Zijian Zhao, Boxun Li, Tete Xiao, Gang Yu, Xiangyu Zhang, and Jian Sun. Crowdhuman: A benchmark for detecting human in a crowd. *arXiv preprint arXiv:1805.00123*, 2018. [1](#), [6](#), [7](#)

- [71] Zheyuan Shen, Peng Cui, Tong Zhang, and Kun Kunag. Stable learning via sample reweighting. In *Proceedings of the AAAI Conference on Artificial Intelligence*, volume 34, pages 5692–5699, 2020. [2](#) [3](#)
- [72] Zheyuan Shen, Jiashuo Liu, Yue He, Xingxuan Zhang, Renzhe Xu, Han Yu, and Peng Cui. Towards out-of-distribution generalization: A survey. *arXiv preprint arXiv:2108.13624*, 2021. [1](#) [2](#) [3](#)
- [73] Abhinav Shrivastava, Abhinav Gupta, and Ross Girshick. Training region-based object detectors with online hard example mining. In *Proceedings of the IEEE conference on computer vision and pattern recognition*, pages 761–769, 2016. [3](#)
- [74] Baichen Sun and Kate Saenko. Deep coral: Correlation alignment for deep domain adaptation. In *European conference on computer vision*, pages 443–450. Springer, 2016. [3](#)
- [75] Baichen Sun and Kate Saenko. Deep coral: Correlation alignment for deep domain adaptation. In *ECCV Workshops*, 2016. [8](#)
- [76] Yu Sun, Eric Tzeng, Trevor Darrell, and Alexei A Efros. Unsupervised domain adaptation through self-supervision. *arXiv preprint arXiv:1909.11825*, 2019. [3](#)
- [77] Zhi Tian, Chunhua Shen, Hao Chen, and Tong He. Fcos: Fully convolutional one-stage object detection. In *Proceedings of the IEEE/CVF international conference on computer vision*, pages 9627–9636, 2019. [2](#)
- [78] A Torralba and AA Efros. Unbiased look at dataset bias. In *Proceedings of the 2011 IEEE Conference on Computer Vision and Pattern Recognition*, pages 1521–1528, 2011. [2](#)
- [79] Riccardo Volpi, Hongseok Namkoong, Ozan Sener, John Duchi, Vittorio Murino, and Silvio Savarese. Generalizing to unseen domains via adversarial data augmentation. *arXiv preprint arXiv:1805.12018*, 2018. [2](#) [3](#)
- [80] Jindong Wang, Cuiling Lan, Chang Liu, Yidong Ouyang, Wenjun Zeng, and Tao Qin. Generalizing to unseen domains: A survey on domain generalization. *arXiv preprint arXiv:2103.03097*, 2021. [2](#) [3](#)
- [81] Wenhao Wang. Adapted center and scale prediction: More stable and more accurate. *arXiv preprint arXiv:2002.09053*, 2020. [2](#) [6](#) [10](#) [15](#)
- [82] Xinlong Wang, Tete Xiao, Yuning Jiang, Shuai Shao, Jian Sun, and Chunhua Shen. Repulsion loss: Detecting pedestrians in a crowd. In *Proceedings of the IEEE Conference on Computer Vision and Pattern Recognition*, pages 7774–7783, 2018. [2](#)
- [83] Enze Xie, Peize Sun, Xiaoge Song, Wenhai Wang, Xuebo Liu, Ding Liang, Chunhua Shen, and Ping Luo. Polarmask: Single shot instance segmentation with polar representation. In *Proceedings of the IEEE/CVF conference on computer vision and pattern recognition*, pages 12193–12202, 2020. [2](#)
- [84] Chang-Dong Xu, Xing-Ran Zhao, Xin Jin, and Xiu-Shen Wei. Exploring categorical regularization for domain adaptive object detection. In *Proceedings of the IEEE/CVF Conference on Computer Vision and Pattern Recognition*, pages 11724–11733, 2020. [3](#)
- [85] Huazhe Xu, Yang Gao, Fisher Yu, and Trevor Darrell. End-to-end learning of driving models from large-scale video datasets. *2017 IEEE Conference on Computer Vision and Pattern Recognition (CVPR)*, pages 3530–3538, 2017. [6](#)
- [86] Renzhe Xu, Peng Cui, Zheyuan Shen, Xingxuan Zhang, and Tong Zhang. Why stable learning works? a theory of covariate shift generalization. *arXiv preprint arXiv:2111.02355*, 2021. [3](#)
- [87] Ze Yang, Shaohui Liu, Han Hu, Liwei Wang, and Stephen Lin. Reppoints: Point set representation for object detection. In *Proceedings of the IEEE/CVF International Conference on Computer Vision*, pages 9657–9666, 2019. [2](#)
- [88] Ze Yang, Yinghao Xu, Han Xue, Zheng Zhang, Raquel Urtasun, Liwei Wang, Stephen Lin, and Han Hu. Dense repoints: Representing visual objects with dense point sets. In *European Conference on Computer Vision*, pages 227–244. Springer, 2020. [2](#)
- [89] Xingyu Yao, Sicheng Zhao, Pengfei Xu, and Jufeng Yang. Multi-source domain adaptation for object detection. In *Proceedings of the IEEE/CVF International Conference on Computer Vision*, pages 3273–3282, 2021. [3](#)
- [90] Xiangyu Yue, Yang Zhang, Sicheng Zhao, Alberto Sangiovanni-Vincentelli, Kurt Keutzer, and Boqing Gong. Domain randomization and pyramid consistency: Simulation-to-real generalization without accessing target domain data. In *Proceedings of the IEEE/CVF International Conference on Computer Vision*, pages 2100–2110, 2019. [3](#)
- [91] Syed Sahil Abbas Zaidi, Mohammad Samar Ansari, Asra Aslam, Nadia Kanwal, Mamoon Asghar, and Brian Lee. A survey of modern deep learning based object detection models. *Digital Signal Processing*, page 103514, 2022. [1](#)
- [92] Liliang Zhang, Liang Lin, Xiaodan Liang, and Kaiming He. Is faster r-cnn doing well for pedestrian detection? In *European conference on computer vision*, pages 443–457. Springer, 2016. [2](#)
- [93] Pengfei Zhang, Cuiling Lan, Wenjun Zeng, Junliang Xing, Jianru Xue, and Nanning Zheng. Semantics-guided neural networks for efficient skeleton-based human action recognition. In *Proceedings of the IEEE/CVF Conference on Computer Vision and Pattern Recognition*, pages 1112–1121, 2020. [1](#)
- [94] Shanshan Zhang, Rodrigo Benenson, Mohamed Omran, Jan Hosang, and Bernt Schiele. How far are we from solving pedestrian detection? In *Proceedings of the iEEE conference on computer vision and pattern recognition*, pages 1259–1267, 2016. [2](#) [6](#)
- [95] Shanshan Zhang, Rodrigo Benenson, and Bernt Schiele. Citypersons: A diverse dataset for pedestrian detection. In *Proceedings of the IEEE Conference on Computer Vision and Pattern Recognition*, pages 3213–3221, 2017. [6](#)
- [96] Shifeng Zhang, Longyin Wen, Xiao Bian, Zhen Lei, and Stan Z Li. Occlusion-aware r-cnn: Detecting pedestrians in a crowd. In *Proceedings of the European Conference on Computer Vision (ECCV)*, pages 637–653, 2018. [2](#)
- [97] Shanshan Zhang, Jian Yang, and Bernt Schiele. Occluded pedestrian detection through guided attention in cnns. In *Proceedings of the IEEE conference on Computer Vision and Pattern Recognition*, pages 6995–7003, 2018. [2](#)

- [98] Xingxuan Zhang, Peng Cui, Renzhe Xu, Linjun Zhou, Yue He, and Zheyen Shen. Deep stable learning for out-of-distribution generalization. In *Proceedings of the IEEE/CVF Conference on Computer Vision and Pattern Recognition*, pages 5372–5382, 2021. 2, 3, 8
- [99] Xingxuan Zhang, Linjun Zhou, Renzhe Xu, Peng Cui, Zheyen Shen, and Haoxin Liu. Domain-irrelevant representation learning for unsupervised domain generalization. *arXiv preprint arXiv:2107.06219*, 2021. 3
- [100] Ganlong Zhao, Guanbin Li, Ruijia Xu, and Liang Lin. Collaborative training between region proposal localization and classification for domain adaptive object detection. In *European Conference on Computer Vision*, pages 86–102. Springer, 2020. 3
- [101] Chunluan Zhou and Junsong Yuan. Bi-box regression for pedestrian detection and occlusion estimation. In *Proceedings of the European Conference on Computer Vision (ECCV)*, pages 135–151, 2018. 2
- [102] Fan Zhou, Zhuqing Jiang, Changjian Shui, Boyu Wang, and Brahim Chaib-draa. Domain generalization with optimal transport and metric learning. *arXiv preprint arXiv:2007.10573*, 2020. 3
- [103] Kaiyang Zhou, Ziwei Liu, Yu Qiao, Tao Xiang, and Chen Change Loy. Domain generalization: A survey. *arXiv preprint arXiv:2103.02503*, 2021. 2, 3
- [104] Kaiyang Zhou, Yongxin Yang, Timothy Hospedales, and Tao Xiang. Learning to generate novel domains for domain generalization. In *European Conference on Computer Vision*, pages 561–578. Springer, 2020. 3
- [105] Xingyi Zhou, Jiacheng Zhuo, and Philipp Krahenbuhl. Bottom-up object detection by grouping extreme and center points. In *Proceedings of the IEEE/CVF conference on computer vision and pattern recognition*, pages 850–859, 2019. 2
- [106] Chenfan Zhuang, Xintong Han, Weilin Huang, and Matthew Scott. ifan: Image-instance full alignment networks for adaptive object detection. In *Proceedings of the AAAI Conference on Artificial Intelligence*, volume 34, pages 13122–13129, 2020. 3
- [107] Zhengxia Zou, Zhenwei Shi, Yuhong Guo, and Jieping Ye. Object detection in 20 years: A survey. *arXiv preprint arXiv:1905.05055*, 2019. 1

A. Appendix

A.1. Detectors Under Distribution Shifts

Table 9. MR^{-2} of detectors trained and tested with the same dataset. All detectors are reimplemented with ResNet-50 [28] pretrained on Imagenet [14] as the backbone. The title of each column indicates the tested subset. The best results of all methods are highlighted with the bold font.

| Model | ECP | | | | CrowdHuman | | | | WiderPedestrian | |
|---------------------|---------------|---------------|---------------|---------------|---------------|---------------|---------------|---------------|-----------------|--|
| | Reasonable | Small | Heavy | All | Reasonable | Small | Heavy | All | All | |
| CrowdDet | 0.0941 | 0.1442 | 0.3899 | 0.3322 | 0.1771 | 0.1835 | 0.4056 | 0.3884 | 0.5329 | |
| LLA | 0.1387 | 0.2093 | 0.4701 | 0.4033 | 0.1944 | 0.2092 | 0.4287 | 0.4096 | 0.5774 | |
| RetinaNet | 0.1674 | 0.2584 | 0.4817 | 0.4692 | 0.2976 | 0.2830 | 0.4907 | 0.5418 | 0.5556 | |
| Faster RCNN | 0.1273 | 0.2017 | 0.4616 | 0.4071 | 0.1912 | 0.2008 | 0.4226 | 0.4025 | 0.5617 | |
| RAPT (ours) + FRCNN | 0.1235 | 0.2253 | 0.4675 | 0.4109 | 0.1920 | 0.2115 | 0.4157 | 0.4079 | 0.5596 | |

As discussed in Section 4, despite the striking performance current pedestrian detectors achieved when trained and tested with a single dataset, they suffer a significant drop under distribution shifts between training and testing data. Here we present the results of detectors trained and tested with a single dataset in Table 9. Compared with results in Table 1, Table 4 and Table 5 in the main paper, detectors trained and tested with a single dataset show significant higher performance on ECP, CrowdHuman and WiderPedestrian, which indicating clear performance drop caused by distribution shifts between training and testing datasets. The results meet observations in previous works [9, 25] and show that distribution shifts is a crucial problem for the real-world applications of pedestrian detectors. Furthermore, RAPT shows no superior performance compared to current detectors, yet shows considerable improvement under distribution shifts.

A.2. More Experimental Results

Table 10. mean Average Precision (mAP) of detectors trained on CrowdHuman and ECP, and tested on CityPersons, Caltech and Wider-Pedestrian. All detectors are reimplemented with ResNet-50 [28] pretrained on Imagenet [14] as the backbone. The title of each column indicates the tested subset. The best results of all methods are highlighted with the bold font.

| Method | Training Data | CityPersons | | | | Caltech | | | | WiderPedestrian | | | |
|---------------------|----------------|--------------|--------------|--------------|--------------|--------------|--------------|--------------|--------------|-----------------|--------------|--------------|--------------|
| | | Small | Medium | Large | All | Small | Medium | Large | All | Small | Medium | Large | All |
| CrowdDet [11] | CrowdHuman+ECP | 0.101 | 0.406 | 0.519 | 0.368 | 0.080 | 0.283 | 0.450 | 0.169 | 0.098 | 0.333 | 0.495 | 0.340 |
| IterDet [67] | CrowdHuman+ECP | 0.068 | 0.372 | 0.463 | 0.328 | 0.041 | 0.213 | 0.407 | 0.119 | 0.061 | 0.242 | 0.339 | 0.231 |
| ACSP [81] | CrowdHuman+ECP | 0.050 | 0.390 | 0.590 | 0.367 | 0.049 | 0.229 | 0.415 | 0.126 | 0.067 | 0.251 | 0.355 | 0.249 |
| LLA [19] | CrowdHuman+ECP | 0.132 | 0.397 | 0.486 | 0.362 | 0.089 | 0.286 | 0.454 | 0.174 | 0.105 | 0.326 | 0.476 | 0.330 |
| RetinaNet [44] | CrowdHuman+ECP | 0.072 | 0.387 | 0.484 | 0.342 | 0.088 | 0.297 | 0.434 | 0.177 | 0.105 | 0.334 | 0.492 | 0.336 |
| Cascade RCNN [6] | CrowdHuman+ECP | 0.070 | 0.378 | 0.472 | 0.339 | 0.042 | 0.217 | 0.412 | 0.123 | 0.062 | 0.247 | 0.348 | 0.238 |
| Faster RCNN [65] | CrowdHuman+ECP | 0.160 | 0.425 | 0.503 | 0.389 | 0.101 | 0.301 | 0.441 | 0.187 | 0.127 | 0.348 | 0.513 | 0.358 |
| RAPT (ours) + FRCNN | CrowdHuman+ECP | 0.156 | 0.433 | 0.515 | 0.403 | 0.112 | 0.325 | 0.437 | 0.193 | 0.112 | 0.353 | 0.499 | 0.368 |

Table 11. Mean Average Precision (mAP) of detectors trained on open-world datasets and tested on autonomous driving ones. For details about the number of runs, meaning of column titles and fonts, see Table 9.

| Model | Training | ECP | | | | Caltech | | | | CityPersons | | | |
|---------------------|----------|--------------|--------------|--------------|--------------|--------------|--------------|--------------|--------------|--------------|--------------|--------------|--------------|
| | | Small | Medium | Large | All | Small | Medium | Large | All | Small | Medium | Large | All |
| CrowdDet | C+W | 0.099 | 0.349 | 0.555 | 0.322 | 0.073 | 0.276 | 0.449 | 0.165 | 0.067 | 0.320 | 0.487 | 0.306 |
| IterDet | C+W | 0.062 | 0.293 | 0.387 | 0.246 | 0.057 | 0.239 | 0.413 | 0.138 | 0.052 | 0.312 | 0.451 | 0.289 |
| LLA | C+W | 0.124 | 0.352 | 0.538 | 0.328 | 0.072 | 0.255 | 0.429 | 0.156 | 0.087 | 0.321 | 0.449 | 0.301 |
| RetinaNet | C+W | 0.096 | 0.354 | 0.548 | 0.321 | 0.073 | 0.270 | 0.421 | 0.161 | 0.057 | 0.324 | 0.463 | 0.298 |
| Cascade RCNN | C+W | 0.071 | 0.302 | 0.393 | 0.255 | 0.061 | 0.246 | 0.422 | 0.144 | 0.056 | 0.318 | 0.458 | 0.294 |
| Faster RCNN | C+W | 0.104 | 0.357 | 0.549 | 0.326 | 0.078 | 0.271 | 0.438 | 0.162 | 0.067 | 0.330 | 0.477 | 0.308 |
| RAPT (ours) + FRCNN | C+W | 0.115 | 0.375 | 0.539 | 0.340 | 0.070 | 0.279 | 0.446 | 0.172 | 0.076 | 0.351 | 0.489 | 0.320 |

We present mean Average Precision (mAP) of detectors trained on CrowdHuman and ECP, and tested on CityPersons, Caltech and WiderPedestrian in Table 10, which shares the same experimental setting with Table 1 in the main paper. We present mean Average Precision (mAP) of detectors trained on CrowdHuman and WiderPedestrian, and tested on ECP, Caltech and CityPersons in Table 11, which shares the same experimental setting with Table 5 in the main paper. The proposed RAPT consistently shows superior mAP on all datasets.

Table 12. MR^{-2} of detectors evaluated under random distribution shifts. For details about the number of runs, meaning of column titles and fonts, see Table 9.

| Model | Training Data | CrowdHuman | | | | WiderPedestrian | COCO |
|-------------------|---------------|---------------|---------------|---------------|---------------|-----------------|---------------|
| | | Reasonable | Small | Heavy | All | | |
| CrowdDet | ECP+Caltech | 0.6806 | 0.6118 | 0.9188 | 0.8367 | 0.8153 | 0.8051 |
| LLA | ECP+Caltech | 0.6548 | 0.6073 | 0.9221 | 0.8350 | 0.8151 | 0.7715 |
| RetinaNet | ECP+Caltech | 0.6968 | 0.6385 | 0.9280 | 0.8580 | 0.8132 | 0.7744 |
| Faster RCNN | ECP+Caltech | 0.6740 | 0.6286 | 0.9242 | 0.8268 | 0.8017 | 0.7927 |
| RAPT (ours)+FRCNN | ECP+Caltech | 0.6651 | 0.6108 | 0.9003 | 0.8173 | 0.7981 | 0.7825 |

A.3. More Bounding Boxes Visualization.

We show more bounding boxes visualization in Figure 4 and Figure 5. RAPT generates more accurate bounding boxes and fewer wrong bounding boxes, indicating a clear improvement of generalization ability under distribution shifts.

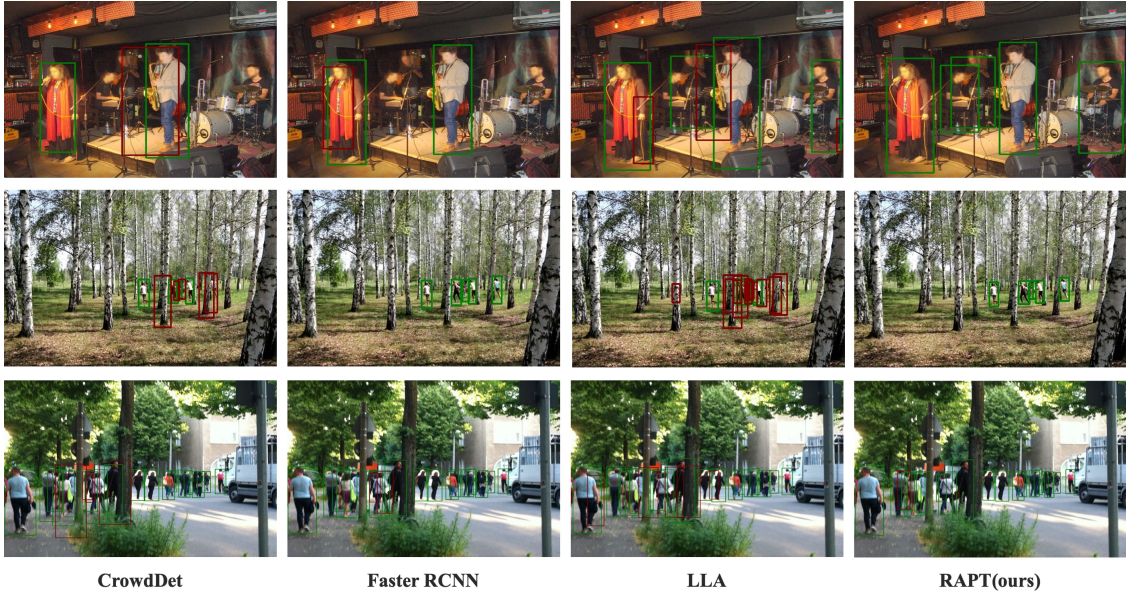


Figure 4. Visualization of bounding boxes detected by RAPT, CrowdDet, LLA and Faster RCNN. RAPT yields less wrong detected bounding boxes (marked with red anchors) compared with CrowdDet and LLA, and more accurate bounding boxes than Faster RCNN.

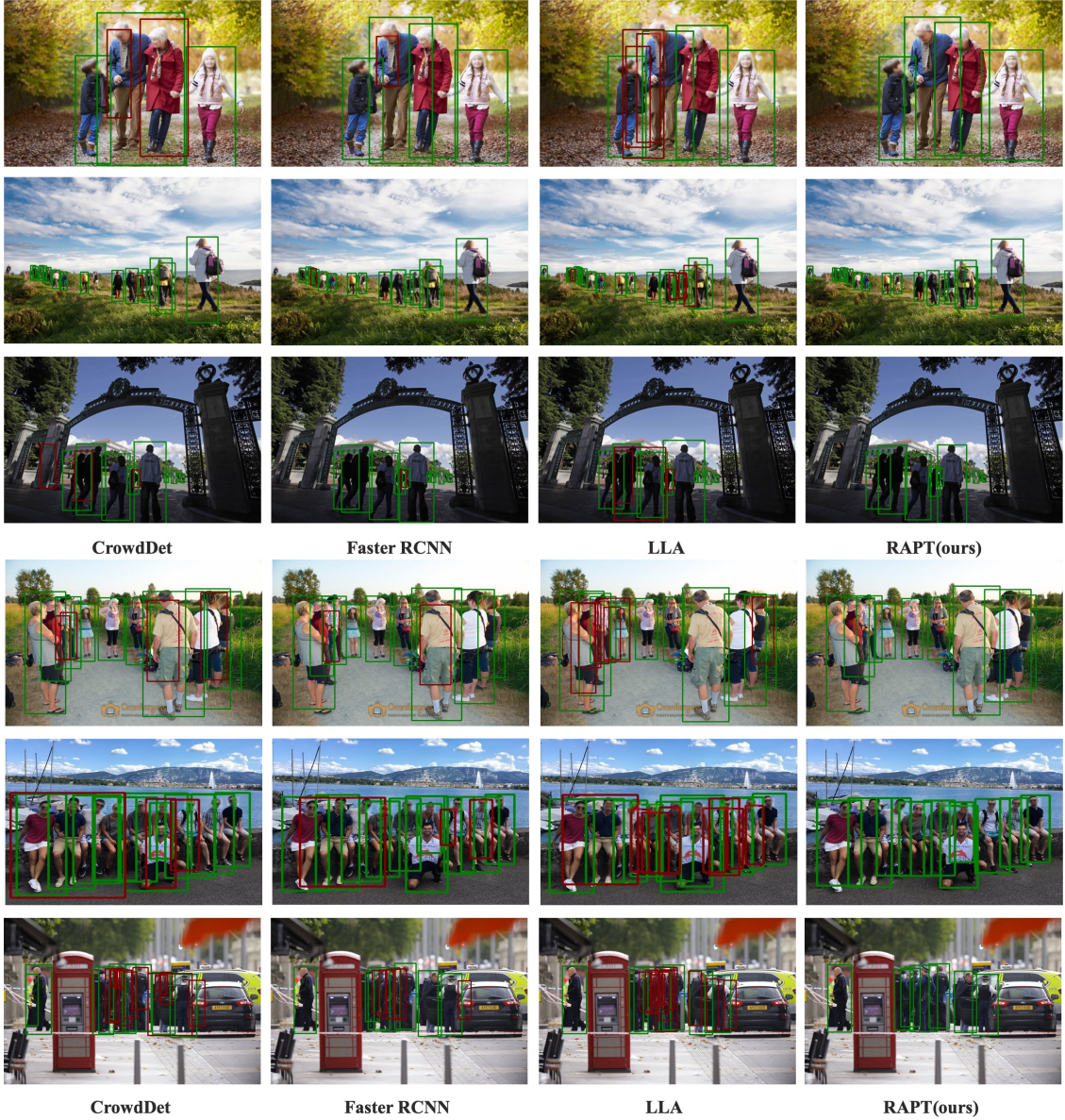


Figure 5. Visualization of bounding boxes detected by RAPT, CrowdDet, LLA and Faster RCNN. RAPT yields less wrong detected bounding boxes (marked with red anchors) compared with CrowdDet and LLA, and more accurate bounding boxes than Faster RCNN.